Molecular-Dynamics Simulations of Cold Antihydrogen Formation in Strongly Magnetized Plasmas

S. X. Hu,* D. Vrinceanu, S. Mazevet, and L. A. Collins

Theoretical Division, Los Alamos National Laboratory, Los Alamos, New Mexico 87545, USA

(Received 9 March 2005; published 12 October 2005)

Employing a high-order symplectic integrator and an adaptive time-step algorithm, we perform molecular-dynamics simulations of antihydrogen formation, in a cold plasma confined by a strong magnetic field, over time scales of microseconds. Sufficient positron-antiproton recombination events occur to allow a statistical analysis for various properties of the formed antihydrogen atoms. Giant-dipole states are formed in the initial stage of recombination. In addition to neutral atoms, we also observe antihydrogen positive ions ($\bar{H}^+$), in which two positrons simultaneously bind to an antiproton.

DOI: 10.1103/PhysRevLett.95.163402 PACS numbers: 36.10.−k, 31.15.Qg, 34.80.Lx

The antihydrogen atom ($\bar{H}$), the simplest form of antimatter, is of fundamental importance in possible high-precision tests of the standard model (*CPT* violation) and of gravity theories of matter and antimatter [1]. Two experimental groups at CERN, ATHENA [2] and ATRAP [3], have recently detected cold $\bar{H}$ atoms produced by mixing antiprotons ($\bar{p}$) with cold positrons (e^+) in a nested Penning trap. Properties of the formed antihydrogen atoms, such as their energy levels, temperature, and spatial distribution, are currently being examined experimentally [4–6]. Knowledge of the state of the formed $\bar{H}$ is crucial to devising deexcitation schemes to low-lying levels, suitable for precision spectroscopy. While the theory of strongly magnetized isolated $\bar{H}$ atoms has been analyzed [7,8] as well as restricted $\bar{H}$ recombination models [9,10], statistics of the properties of $\bar{H}$ formed within full dynamics plasma simulations are lacking. In this Letter, we present comprehensive studies on recombined $\bar{H}$ using molecular-dynamics (MD) simulations of cold $\bar{p}$-e^+ plasmas in a strong magnetic field. Employing a high-order symplectic integrator [11] and an adaptive time-step algorithm, we model plasmas of 5000 to 10 000 particles for very long times (~ 1 μs). We observe sufficient recombination events that enable us to extract the statistical properties of $\bar{H}$.

In order to model the experimental conditions [2,3], a plasma of $\bar{p}$ (with mass m_p and charge $-e$) and e^+ (with mass m_e and charge $+e$) is simulated in cylindrical geometry with a constant magnetic field ($B = 5.4$ T) oriented along the z axis. A typical cylindrical region with a radius of 85 μm and an axial length of 2202 μm is uniformly populated with $4000e^+$'s and $1000\bar{p}$'s, for most simulations. This arrangement gives a positron density $\sim 8 \times 10^7$ cm^{-3}, which corresponds to experimental conditions. All particles are initially placed at random positions within the cylindrical volume. The longitudinal velocities (along the z axis) of e^+ are chosen according to a 4 K Maxwell-Boltzmann distribution, while their transverse velocities (in the xy plane) are $(\hbar eB)^{1/2}/m_e$, assuming that all e^+ are in their ground Landau state. The longitudinal velocity of the $\bar{p}$ is an input parameter for our simulations. The transverse velocities are all equal in magnitude to the longitudinal velocity and oriented according to a random phase, which describes the initial position of the gyration radius on the cyclotron orbit. This special way of choosing the initial conditions simulates the experimental setup used by the ATRAP experiment [3], where the $\bar{p}$'s are driven through the e^+ cloud using a radio-frequency pulse.

Starting from these initial conditions, the evolution of the particles is integrated according to the classical equations of motion. Because of the strong transverse confinement, mirror-boundary conditions are imposed only along the z axis. Particles reaching the end caps are reflected back into the cylinder by flipping the longitudinal component of their velocity. We employ a special fourth-order symplectic integrator [11], which can take advantage of the low density of the plasma. Unless a very rare close encounter occurs, the long-range Coulomb interaction can be treated as a perturbation of the cyclotron motion of the charged particles in the strong magnetic field. Each time step consists of two stages ("drift" and "kick"). During a drift stage, particle coordinates are propagated according to their cyclotron motion, ignoring their Coulomb interaction. The Coulomb forces change instantaneously the momentum of each particle at the kick stage. A very long integration time (up to 1 μs) has been obtained in this way. In order to deal with the close encounter collisions and speed up simulations, we use an adaptive algorithm by which the time step is adjusted to maintain the error in energy conservation under 1% of the system energy at all times during the simulations. The transverse cyclotron motion is preserved, similar to the guiding-center approximation [12], but at every time step and not globally.

We first present results from a simulation with an initial $\bar{p}$ kinetic energy $E_p = 23.2$ K (~ 2 meV). In Fig. 1, we plot the minimum distance between a $\bar{p}$ and its nearest e^+ as a function of time, up to the total simulation time of 0.5 μs. The panels in Fig. 1 present four representative cases of various $\bar{p}$-e^+ pairs. From Fig. 1(a), we see that the minimum $\bar{p}$-e^+ distance varies rapidly and irregularly

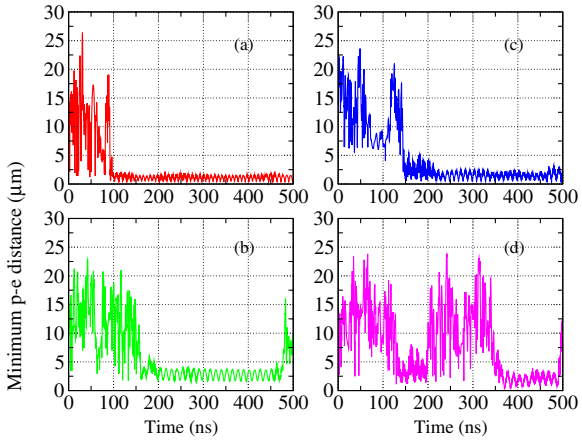

FIG. 1 (color online). The minimum distance between a $\bar{p}$ and its nearest e^+ as a function of time, for four different situations.

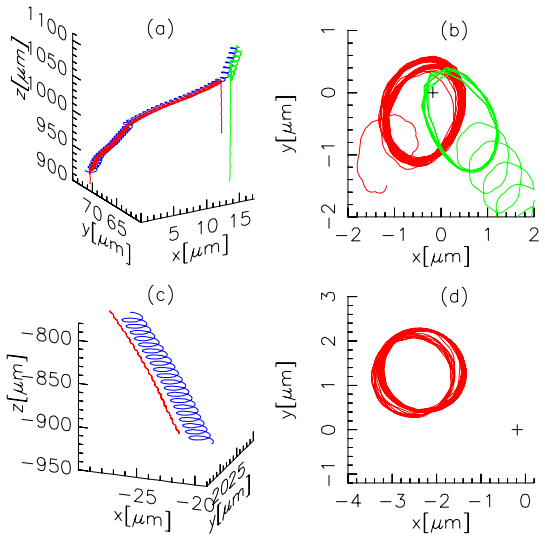

FIG. 2 (color online). The trajectories for recombined pairs shown in Figs. 1(a) and 1(b). The $\bar{p}$ are plotted in lines with large cyclotron radius in (a) and (c), and with black crosses in (b) and (d), while e^+ are indicated by lines with small cyclotron radius.

from 2 to 25 μm during the first 0.1 μs; it then exhibits regular oscillations from $t = 0.1$ to 0.5 μs. Checking the specific identity of the e^+, we find that it does not change from $t \simeq 0.1$ μs to $t \simeq 0.44$ μs. This regular oscillation in the minimum $\bar{p}$-e^+ distance provides a "signature" of recombination of e^+ with $\bar{p}$. A simple criterion for defining a recombination event is then to require that the $\bar{p}$-e^+ pair "sticks" together for more than a certain amount of time. We have chosen 50 ns since during this period several oscillations in the minimum $\bar{p}$-e^+ distance are apparent. Another criterion based on axial binding energy is also used and gives the same set of recombination events. For the other panels in Fig. 1, we find that the formed pairs ($\bar{\mathrm{H}}$) can be destroyed or ionized [in 1(b) at $t \simeq 480$ ns], deexcited [in 1(c) at $t \simeq 200$ ns], and recombined again [in 1(d) at $t \simeq 350$ ns] in the plasma. By examining the detailed dynamics of the formation of $\bar{p}$-e^+ pairs, we found that the dominant process is three-body recombination, although replacement collisions (discussed below) can possibly occur.

The detailed trajectories for the recombined pairs shown in Figs. 1(a) and 1(b) are further examined in Fig. 2. Figures 2(a) and 2(b) represent the situation of Fig. 1(a), while the Figs. 2(c) and 2(d) are for the case of Fig. 1(b). The 3D trajectory plots 2(a) and 2(c) elucidate the attachment of the e^+ (lines showing small cyclotron radii) with the $\bar{p}$ (line showing large cyclotron radius), in which the combined $\bar{p}$-e^+ are traveling together for more than 200 μm in the plasma. The large cyclotron motion of $\bar{p}$ is distinctive. Interestingly, Fig. 2(a) shows a "replacement collision" occurring at $t \sim 0.44$ μs, when a second positron (green line) collides with the $\bar{\mathrm{H}}$ and subsequently replaces the originally recombined positron (red line). To further confirm that the particles are really recombined, we checked their z coordinate against time and clearly found that these ($\bar{p}$-e^+) pairs are moving together along the magnetic field line during the recombination times. Figures 2(b) and 2(d) show the projection of e^+ trajectories in the perpendicular xy plane relative to $\bar{p}$ (black cross) located at the origin. The e^+ in 2(b) is moving (drifting) around the $\bar{p}$, corresponding to a tight bound $\bar{\mathrm{H}}$ in the inner Coulomb well of the $\bar{p}$-e^+ effective potential (defined in [7]). A totally different situation is presented in 2(d) where e^+ oscillates in a well displaced from $\bar{p}$, forming a "giant-dipole" $\bar{\mathrm{H}}$ atom [7]. In Fig. 2(b) we are plotting the trajectory for times from $t = 0.1$ to 0.5 μs so that we see the first e^+ (left circle) leaves its stable trajectory, when the second e^+ (right circle) starts to orbit the $\bar{p}$.

To find the optimal velocity for recombination when $\bar{p}$'s are driven through the e^+ cloud, we simulate plasmas with different initial $\bar{p}$ kinetic energy (E_p). Figure 3(a) shows the number of recombined $\bar{p}$-e^+ pairs as a function of simulation time, for the case of $E_p = 23.2$ K. The number of $\bar{\mathrm{H}}$ atoms fluctuates around 12 events after $t > 0.2$ μs, which indicates the continuous recombination and destruction of $\bar{\mathrm{H}}$ occurs during the $\bar{p}$-e^+ plasma evolution (i.e., the lifetime of each recombined pair varies). A total number of 62 recombination events have been counted during the 0.5 μs simulation period. In Fig. 3(b) we display the total number of recombination events ($\bar{\mathrm{H}}$) as a function of the initial $\bar{p}$ kinetic energy (E_p). According to their perpendicular motion (on the xy plane), we further divide these $\bar{\mathrm{H}}$ into two types: the giant-dipole and the "non-giant-dipole," as indicated by examples in Figs. 2(d) and 2(b), respectively. Note that the non-giant-dipole-type $\bar{\mathrm{H}}$ atoms are not necessarily tightly bound; they may have large orbits. The recombination depends only slightly on the $\bar{p}$ energy and has a peak between $E_p = 20$ and 50 K, followed by a slow decrease at large $\bar{p}$ energies. The recombination rates (typically $\approx 10^5$ s^{-1}) obtained in our simulations are about 2 orders of magnitude larger than the rates predicted by bottleneck theories [10,13]. This is because our simulations describe only the collisional capture—the initial phase of recombination in a cold plasma. A much

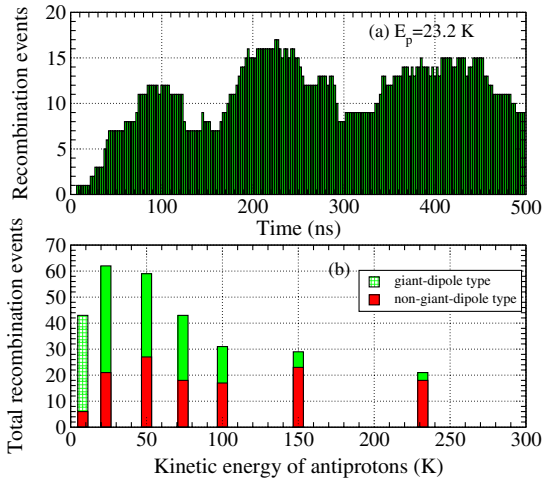

FIG. 3 (color online). (a) The time dependence of $\bar{H}$ recombination for the case of initial $\bar{p}$ energy $E_p = 23.2$ K. (b) The total $\bar{H}$ recombination events (during 0.5 μs) as a function of the initial kinetic energy (E_p) of antiprotons (in units of K).

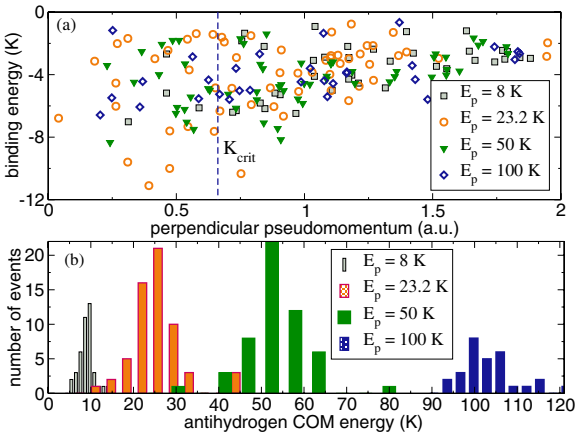

FIG. 4 (color online). Perpendicular pseudomomenta and binding energies (a) and time-averaged kinetic energies (b) of $\bar{H}$ atoms formed in simulations started with $\bar{p}$ energies of 8, 23.2, 50, and 100 K.

longer simulation time would allow one to observe the stabilization of recombination, for the positron densities considered.

As shown in [7], while the total momentum of $\bar{H}$ atoms is not conserved, the pseudomomentum $\mathbf{K} = M\mathbf{V} - e\mathbf{r} \times \mathbf{B}$ is. Here $M = m_e + m_p$ is the total mass, $\mathbf{V}$ is the center of mass (c.m.) velocity, and $\mathbf{r}$ is the relative distance between the two particles. The perpendicular component $K_\perp$ characterizes the effective potential between $\bar{p}$ and e^+ in a strong magnetic field. When $K_\perp$ is greater than a critical value $K_{\rm crit}$, large giant-dipole states are possible in the outer well [7]. Figure 4(a) shows the distribution of pseudomomenta and binding energies for $\bar{H}$ atoms formed in simulations started with various $\bar{p}$ velocities. Because of the coupling between the relative and c.m. degrees of freedom, a strict definition for the binding energy is not possible. However, the axial relative energy gives a good indication of the binding, because the $\bar{p}$-e^+ pair breaks when particles separate along the field axis. We calculate the binding energy as $W_{\bar{H}} = \mu v_z^2/2 - e^2/\sqrt{z^2 + r_g^2}$, with the reduced mass $\mu = m_e m_p/(m_e + m_p)$, the relative axial distance z and velocity v_z along the magnetic field, and the guiding-center separation r_g. While $\bar{H}$ is bound, the binding energy $W_{\bar{H}}$ is always negative and fluctuates, having maxima when the guiding-center separation is largest. The average value of $W_{\bar{H}}$ at those peaks is our working definition for the binding energy.

As is shown in Fig. 4(a), most $\bar{H}$ atoms formed in our simulations have a binding energy of $\sim$4 K. This is consistent with the prediction of the "bottleneck theory" [10,13], which states that the probable binding energy in a three-body recombination process is approximately equal in magnitude to the thermal energy of positron cloud (always 4 K in our simulations). Figure 4(a) also shows that deeply bounded pairs are possible only for small values of $K_\perp$. Numerous $\bar{H}$ atoms have pseudomomenta greater than $K_{\rm crit} = 0.658$ a.u., indicating that they are of either the giant-dipole type or the large non-giant-dipole type.

The kinetic energies of $\bar{H}$ atoms, calculated as the average of the c.m. energy over their recombination time, are displayed in Fig. 4(b). The heavy $\bar{p}$ cannot considerably change its velocity in collisions with the lighter e^+, and therefore the kinetic energies of formed $\bar{H}$ atoms are distributed around the $\bar{p}$ energies with which the simulations were started. This also suggests that recombination occurs well before the thermal equilibrium of $\bar{p}$ with e^+ in the plasma, which agrees with the most recent observation in experiments [6]. However, a recent measurement of $\bar{H}$ velocity [5] indicated a "speeding-up" factor of 20, based on the assumption of $\bar{p}$ at 4.2 K. From our simulation results, we believe that the $\bar{p}$ in that experiment were not in thermal equilibrium at 4.2 K, but rather have a much higher temperature $\sim$2000 K.

Next, we calculate the size of $\bar{H}$, designated r, as the time-averaged separation between $\bar{p}$ and e^+. The r distributions of $\bar{H}$ atoms are shown in Fig. 5 for different positron densities: (a) $1.6 \times 10^7/\text{cm}^3$, (b) $8 \times 10^7/\text{cm}^3$ and (c) $4 \times 10^8/\text{cm}^3$, respectively. All these cases are from MD simulations with 5000 particles, up to the same time $T = 0.5$ μs but for different cylinder lengths. The clear feature, elucidated by Fig. 5, is that the $\bar{H}$ size becomes smaller as the plasma density increases. This shows both the deexcitation due to plasma collisions and the lowering of the recombination threshold. We observed that the total number of recombined atoms (living longer than 50 ns) decreases from 71 in low-density plasma [Fig. 5(a)] to 59 and 10 for the other two cases in Figs. 5(b) and 5(c), respectively. This implies that frequent collisions are also considerably ionizing and destroying $\bar{H}$. For the conditions we explored, the smallest $\bar{H}$ has a size of $\sim$1 μm.

Finally, we tested our simulation results for different particle numbers and simulation times as follows: (1) we

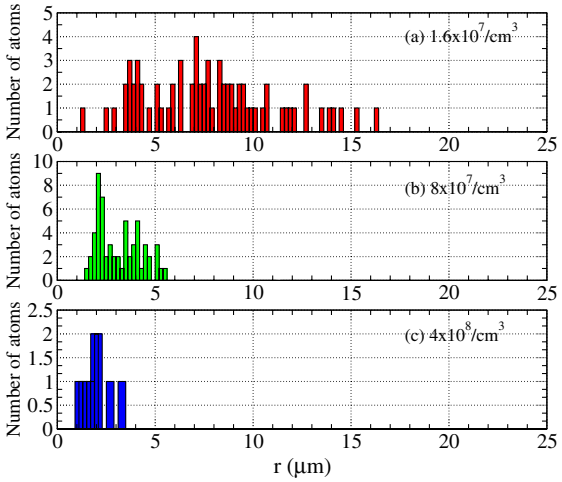

FIG. 5 (color online). The statistics on the formed $\bar{H}$ size, for different positron densities: (a) $1.6\times10^7/\mathrm{cm}^3$, (b) $8\times10^7/\mathrm{cm}^3$, and (c) $4\times10^8/\mathrm{cm}^3$.

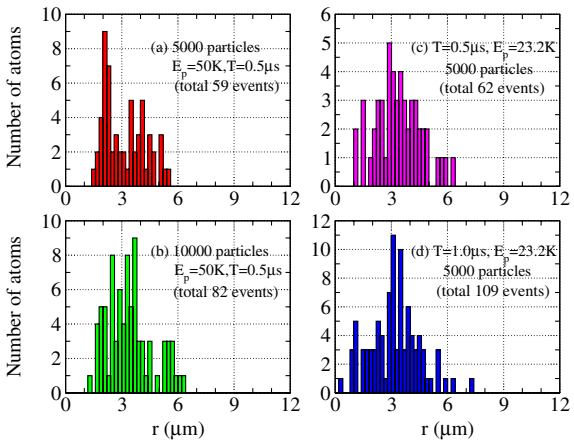

FIG. 6 (color online). The comparison of $\bar{H}$ size distributions: (a) and (b) represent the comparison of results for 5000 and 10 000 particles; while (c) and (d) are for the same 5000 particles but different simulation times ($T = 0.5$ and 1.0 μs).

increased the number of particles to 10 000 ($8000e^+ + 2000\bar{p}$) and lengthened the cylinder by a factor of 2 (in order to keep the same positron density), for which we carry out the MD simulation to the same time 0.5 μs; (2) we kept the original 5000 particles but simulated the plasma up to 1.0 μs. In the first case, the mirror-boundary effect is also examined. For both cases we obtained more recombination events. However, the general properties of formed $\bar{H}$ atoms were statistically unchanged when compared to the corresponding cases having either less particles or shorter simulation time. As an example, we compare the statistics of $\bar{H}$ size distribution in Fig. 6. Figures 6(a) and 6(b) represent the case of changing the number of particles, while Figs. 6(c) and 6(d) represent the comparison between short-time ($T = 0.5$ μs) and long-time ($T = 1.0$ μs) simulations. We also find similar statistical results for other $\bar{H}$ properties, such as kinetic energy, lifetime, and binding-energy distribution. Thus, we believe that the results presented here generally hold as both the number of particles and the simulation times increase. In addition, they do not significantly depend on the choice of the recombination criterion. The statistics were the same when we reduced the $\bar{p}$-e^+ sticking time threshold from 50 to 25 ns.

Besides the mirror-boundary simulations discussed above, we also did some simulations under free expansion, i.e., no boundary. We found 10 times more recombination events as compared to the corresponding mirror-boundary case, in which we also observed antihydrogen positive ions $\bar{H}^+$. Both positrons in $\bar{H}^+$ move in orbits delocalized from the antiproton, in contrast to the magnetized ions discussed in [14], where an outer e^+ is bound by a polarized core. Although they may be weakly bound, $\bar{H}^+$ can have important implications for trapping and manipulating by external fields, since they are charged. Further studies on $\bar{H}^+$ will follow.

In summary, we have simulated the formation of cold $\bar{H}$ atoms in strongly magnetized $\bar{p}$-e^+ plasmas. Detailed trajectory analysis and statistics show the following: (a) the most $\bar{H}$ atoms initially formed by collisional capture are in highly excited states and are strongly polarized by their transverse motion; (b) maximum recombination events are obtained at the initial $\bar{p}$ energy $E_p \approx 20$–50 K; (c) $\bar{H}$ atoms typically have a size of few μm and become smaller when the positron density is increased; and (d) $\bar{H}^+$ can be formed in free expansions of initially mixed non-neutral $\bar{p}$-e^+ plasmas.

This work was performed under the auspices of the U.S. Department of Energy through the Los Alamos National Laboratory under the LDRD-PRD program.

*Electronic address: suxing@lanl.gov

[1] G. Gabrielse, Adv. At. Mol. Opt. Phys. **45**, 1 (2001); M. Niering *et al.*, Phys. Rev. Lett. **84**, 5496 (2000); R. Bluhm, V. A. Kostelecky, and N. Russell, Phys. Rev. D **57**, 3932 (1998); G. Gabrielse, Hyperfine Interact. **44**, 349 (1988).
[2] M. Amoretti *et al.*, Nature (London) **419**, 456 (2002).
[3] G. Gabrielse *et al.*, Phys. Rev. Lett. **89**, 213401 (2002).
[4] G. Gabrielse *et al.*, Phys. Rev. Lett. **89**, 233401 (2002).
[5] G. Gabrielse *et al.*, Phys. Rev. Lett. **93**, 073401 (2004).
[6] N. Madsen *et al.*, Phys. Rev. Lett. **94**, 033403 (2005).
[7] D. Vrinceanu *et al.*, Phys. Rev. Lett. **92**, 133402 (2004).
[8] S. G. Kuzmin and T. M. O'Neil, Phys. Rev. Lett. **92**, 243401 (2004).
[9] F. Robicheaux and J. D. Hanson, Phys. Rev. A **69**, 010701 (2004); F. Robicheaux, Phys. Rev. A **70**, 022510 (2004).
[10] M. E. Glinsky and T. M. O'Neil, Phys. Fluids B **3**, 1279 (1991).
[11] H. Yoshida, Phys. Lett. A **150**, 262 (1990).
[12] S. G. Kuzmin, T. M. O'Neil, and M. E. Glinsky, Phys. Plasmas **11**, 2382 (2004).
[13] M. Mansbach and J. Keck, Phys. Rev. **181**, 275 (1969).
[14] D. H. E. Dubin, Phys. Rev. Lett. **92**, 195002 (2004).